Eur Phys J C **32**, s02, s165–s177 (2004)
Digital Object Identifier (DOI) 10.1140/epjcd/s2003-01-0013-5

EPJ C direct
electronic only

Particle identification with the ALICE TOF detector at very high particle multiplicity

ALICE TOF Group (Bologna-CERN-ITEP-Salerno):
A.N. Akindinov[4], A. Alici[1,2], F. Anselmo[2], P. Antonioli[2], Y.W. Baek[3,6], M. Basile[1,2], G. Cara Romeo[2], E. Cerron-Zeballos[3,6], L. Cifarelli[1,2], F. Cindolo[2], F. Cosenza[5], A. De Caro[5], S. De Pasquale[5], A. Di Bartolomeo[5], M. Fusco Girard[5], V. Golovine[4], M. Guida[5], D. Hatzifotiadou[2], A.B. Kaidalov[4], S.M. Kiselev[4], G. Laurenti[2], E. Lioublev[4], M.L. Luvisetto[2], A. Margotti[2], A.N. Martemiyanov[4], S. Morozov[3,6], R. Nania[2], P. Otiougova[3,6], A. Pesci[2], F. Pierella[1,2], P.A. Polozov[4], E. Scapparone[2], G. Scioli[1,2], S. Sellitto[5], A.V. Smirnitski[4], M.M. Tchoumakov[4], G P. Vacca[2], G. Valenti[2], G. Venturi[1,2], D. Vicinanza[5], K.G. Voloshin[4], M.C.S. Williams[2], S. Witoszynskyj[3,6], B.V. Zagreev[4], C. Zampolli[1,2], and A. Zichichi[1,2]

[1] Dipartimento di Fisica dell'Università, Bologna, Italy
[2] INFN, Bologna, Italy
[3] CERN, Geneva, Switzerland
[4] Institute for Theoretical and Experimental Physics, Moscow, Russia
[5] Dipartimento di Fisica "E.R.Caianiello" dell'Università and INFN, Salerno, Italy
[6] World Laboratory, Lausanne, Switzerland

Received: 4 Aug 2003 / Accepted: 13 Sep 2003 /
Published Online: 13 Oct 2003 –

Abstract. A procedure developed to achieve particle identification in very high multiplicity conditions using a complex time-of-flight system is illustrated in detail by simulating and studying the performance of the ALICE TOF detector in a realistic scenario of Pb-Pb and p-p interactions at LHC.

1 Introduction

ALICE (A Large Ion Collider Experiment) [1] is an experiment at the CERN Large Hadron Collider (LHC), optimized for the study of Pb-Pb collisions, at a centre-of-mass energy of 5.5 TeV per nucleon pair. The prime aim of the experiment is to study in detail the behaviour of nuclear matter at extreme densities and temperatures. The most striking expected phenomenon is a QCD phase transition of nuclear matter into a deconfined state of quarks and gluons, i.e. the QGP (Quark-Gluon-Plasma) state, with chiral symmetry restoration and quark masses reduced to the small bare ones. This QGP will presumably undergo a fast dynamical evolution into a dilute final hadronic state. To understand how collective phenomena and macroscopic properties with many degrees of freedom in the domain of strong (nuclear) interactions emerge from the microscopic laws of subnuclear physics is the challenge of ALICE. This relies on a large number of observables [2], in particular:

- particle multiplicities
- particle spectra (chemical and kinetic freeze-out, temperature and collective flow, hadron yields and chemical composition, elliptic flow and early pressure)
- particle correlations (Hanbury Brown-Twiss radii, intercept parameter, space-time information from radii and dynamics, lifetime of the collision, final state interactions, phase-space density, spin densities)
- jets
- fluctuations
- direct photons
- heavy-quarks and quarkonia
- coherent ultraperipheral phenomena.

The LHC (Pb-Pb) running programme will enable the exploration of this new nuclear and subnuclear physics field, with respect to the presently ongoing RHIC (Au-Au) running, with a factor of 28 jump in centre-of-mass energy and a factor of 4.5-12 jump in multiplicity and energy densities.

The particle identification (PID) power of a very large time-of-flight (TOF) system covering the central rapidity region ($|y| \leq 1$) is of crucial importance in the ALICE experiment. Pion/kaon/proton separation for the bulk of charged particles in the intermediate momentum range (up to a few GeV/c) will provide an essential tool of investigation for most of the relevant physics observables listed above. Some of the basic physics motivations for the ALICE TOF detector have been outlined elsewhere [1,3,4,5].

The large-coverage, powerful TOF detector we envisage building (see Fig. 1) should efficiently operate under severe multiplicity conditions. It should have an excellent intrinsic response and a low overall occupancy at the highest envisaged charged particle density. Present-

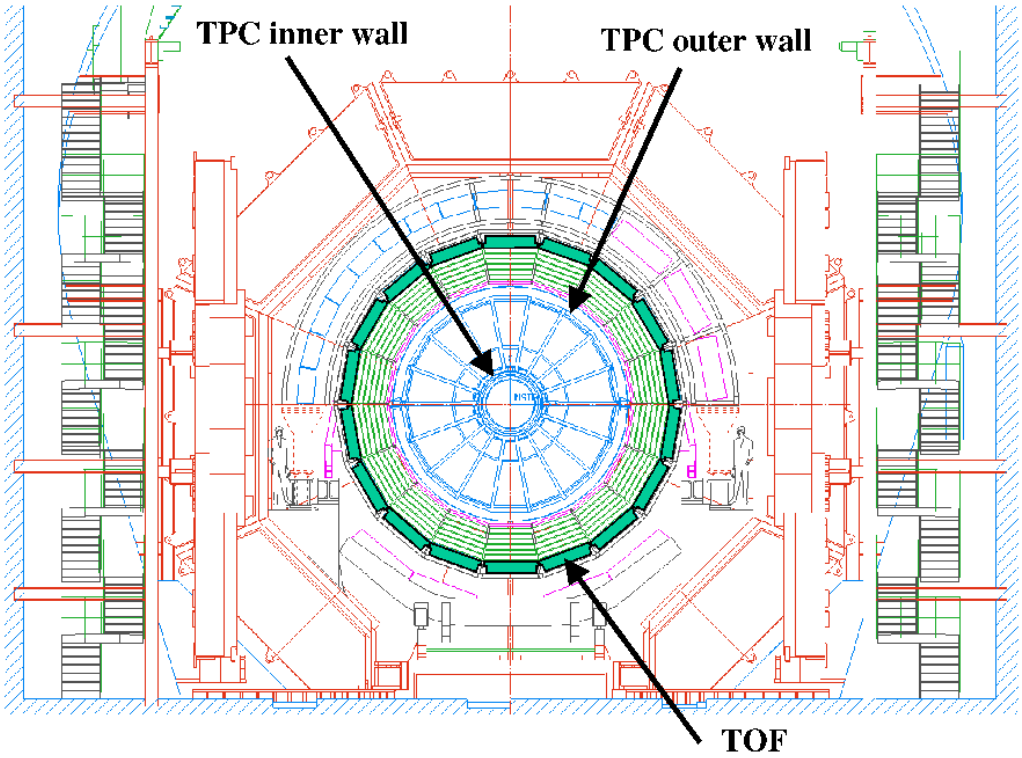

Fig. 1. Transverse view of the ALICE detector, where the 18 sectors of the TOF system can be seen. The inner and the outer walls of the TPC are indicated.

day extrapolations from recent charged-particle multiplicity measurements performed at RHIC in Au-Au collisions at $\sqrt{s} = 130$ GeV per nucleon pair are model dependent and affected by wide uncertainties. Hence dN_{ch}/dy in Pb-Pb at LHC could range from 3000 up to 8000 [2].

The ALICE TOF will be a barrel detector with, as basic element, the double-stack MRPC (Multigap Resistive Plate Chamber) strip. Each strip is equipped with a mosaique of individual readout pads, thus making the TOF barrel a large-coverage, high-granularity hodoscope. The strips are grouped into modules and tilted in space in order to minimize the traversal path for particles coming from the interaction vertex (Fig. 2).

The outstanding features of such a detector in terms of efficiency, time accuracy and rate capability have been extensively described elsewhere [3,4,5]. The main ALICE TOF parameters are:

- radius: $r_{TOF} = 3.7$ m; length: $l_{TOF} = 7.4$ m;
- overall thickness: 30 cm, i.e. 20% of X_0;
- polar-angle coverage: $45° \leq \theta \leq 135°$; full ϕ coverage;
- total number of modules: 90, i.e. 18 (along ϕ) x 5 (along θ);
- total number of MRPC strips: 1638, with 15-19 strips/ module;
- total number of readout pads: 157248, with 2 x 48 readout pads/strip;
- total surface: ≈ 170 m^2; total sensitive surface: ≈ 150 m^2; sensitive area/strip: 7.4 x 122 cm^2; individual readout pad size: 2.5 x 3.5 cm^2;
- dead space: $\approx 10\%$ of total surface;

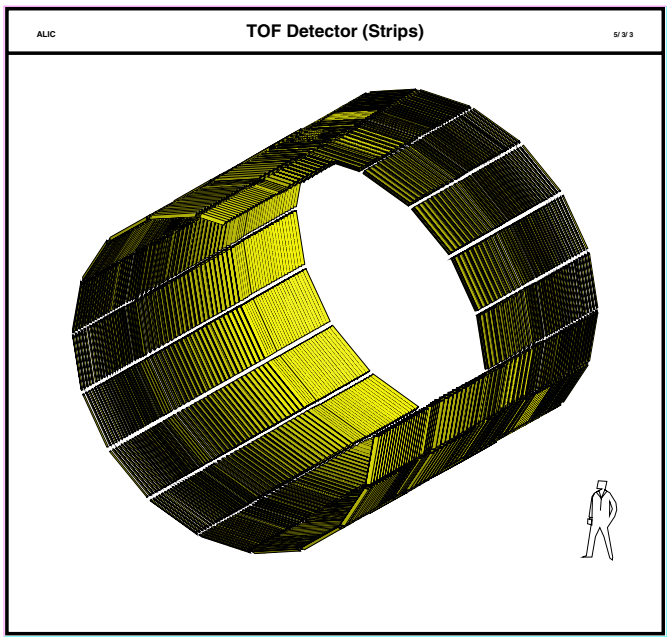

Fig. 2. TOF detector layout in AliROOT where the tilted MRPC strips are visible.

- intrinsic MRPC time resolution: 50-60 ps; overall time resolution: 120 ps (including all other additional sources of time jitter);
- intrinsic MRPC efficiency: 99%.

The ALICE TOF will operate in the presence of a solenoidal magnetic field directed along the beam axis, with B = 0.2-0.5 T. A charged particle density $dN_{ch}/dy = 8000$ at $B = 0.2$ T [3,4,5] represents the most "prohibitive" conditions. In a single SHAKER-generated event [1,3], corresponding to a central Pb-Pb collision, these lead to 12000 charged primary particles produced in the TOF detector angular acceptance, out of which 45% only reach the TOF surface, due to magnetic field, decays and interactions.

On the other hand, a lot of secondaries are produced, resulting in a very high background level. The total number of fired pads (i.e. producing signals) is about 25000 which corresponds to a detector occupancy of $\approx 15\%$. Yet, only 25% of these pads are fired by particles which can be reconstructed in the ALICE TPC (Time Projection Chamber) [6].

Moreover, there is a significant spatial gap between the TPC and the TOF ($r_{TOF} - r_{TPC} = 1.2$ m) which is filled by the ALICE TRD (Transition Radiation Detector) [7], thus causing a high track deviation due to multiple scattering. This tangles the task of matching the TPC-reconstructed tracks with the corresponding pads of the TOF detector.

In this paper we will describe both the TPC-TOF track matching and PID procedures developed so far in order to evaluate the performance of the ALICE TOF system. These methods, tested via Monte Carlo simulations, are already satisfactory although they do not represent an ultimate solution mainly because the TRD is simply treated as passive material. This detector will have in fact some tracking capability (not considered herein) which will likely help improving the TPC-TOF track extrapolation. However these procedures are of general validity and could be applied to other experimental contexts.

The AliROOT package [8] (developed within the framework of the ALICE Software Project) was used in all the calculations discussed in the following. The package is based on ROOT [9] and GEANT3 [10]. It will allow using the same environment in the simulation, reconstruction and analysis stages of the experiment. AliROOT is interfaced with several event generators (JETSET [11], PYTHIA [12], HIJING [13], SHAKER [1], [3], etc.), thus providing a complete set of instruments to fully simulate nucleus-nucleus (or proton-proton) collisions.

2 Track matching

Matching the information acquired by the TOF with the tracking data of the TPC can be done using the so-called "probe-track method" described herein.

In our simulations [3,4,5] all particles generated in the Pb-Pb final state are tracked in the detector using GEANT3. A charged (primary or secondary) particle impinging on the TOF sensitive surface across a given pad produces, with a given efficiency (ε_{eff}), a time signal corresponding to its flight time. This time is smeared according to the overall TOF resolution (σ_{TOF}). The values $\varepsilon_{eff} = 99\%$ and $\sigma_{TOF} = 120$ ps have been used in the present exercise [5]. Hence the TOF detector is set in each event with a number of fired pads. In order to simulate the effect of track reconstruction and fitting in the TPC[1], the GEANT3 information about track position and momentum at the outer layer of the TPC is smeared with the following errors: $\sigma_\phi = 2$ mrad, $\sigma_\theta = 2$ mrad, $\sigma_p/p = 2.1\%$, $\sigma_z = 0.77$ mm, $\sigma_{r_\phi} = 0.62$ mm. The momentum dependence of the TPC tracking errors has been also included [5]. The reconstruction efficiency has been assumed to be 100% (the actual value being $\approx 90\%$).

For each particle tracked/reconstructed in the TPC (called "TPC track" in the following), a statistically significant sample of probe tracks is generated and extrapolated in the magnetic field from the TPC to the TOF. The origin of these probe tracks is set at the outermost end-point of the "mother"-particle track in the TPC (corresponding to a hit in the last TPC pad row). At the TPC end-point, the probe tracks deviate from the mother track according to a Gaussian distribution with standard deviation given by θ^{rms}_{plane}, the mean deflection angle due to multiple scattering[2] through the outer wall of the TPC, the whole TRD and the inner wall of the TOF (corresponding to $\approx 6\%$, 14% and 1% of X_0, respectively). The overall multiple scattering effect is attributed at once to each probe track and a unique tracking step is performed from the TPC to the TOF. No energy loss is considered for the probe tracks, which is a valid approximation here since the multiple scattering effect is dominant.

The number of probe tracks per mother track (N_{probe}) must be adequate (the larger θ^{rms}_{plane}, the larger this number should be). We have chosen here $N_{probe} = 20$, as a good compromise between statistical requirements and CPU time. Therefore a shower of probe tracks is associated in this way to each TPC track.

Every probe track can cross a TOF pad (or a TOF dead region) and be assigned a weighting contribution: $weight_1 = \epsilon_{eff}$ if the sensitive pad hit has fired, $weight_1 = 1-\epsilon_{eff}$ if the sensitive pad hit has not fired. A schematic view of the probe-track shower is shown in Fig. 3. This is a simplified picture since, as already mentioned, the TOF surface inside each module is not planar but made of an arrangement of tilted strips.

A particle crossing a TOF pad can sometimes induce a small signal also on the neighbouring pad(s) and this signal can be slightly delayed (the lower the charge induced, the longer the delay). In order to minimize this effect, to each fired pad we assign an additional weighting factor, $weight_2 = q^2_{induced}$, where $q_{induced}$ is the (normalized)

[1] A Kalman filtering procedure has been recently implemented for track finding and reconstruction in the ALICE TPC and ITS (Inner Tracking System) [14], the latter being a silicon vertex detector surrounding the beam pipe. In ref. [15] some preliminary results have been obtained concerning the extension of this Kalman filter to the TOF, with an option to include the TRD as a tracking device.

[2] Here the pion mass is assumed for all tracks. By taking advantage of the particle identification provided by the TPC (using dE/dx measurements), a more accurate value of θ^{rms}_{plane} could be derived, whenever possible, at low momenta.

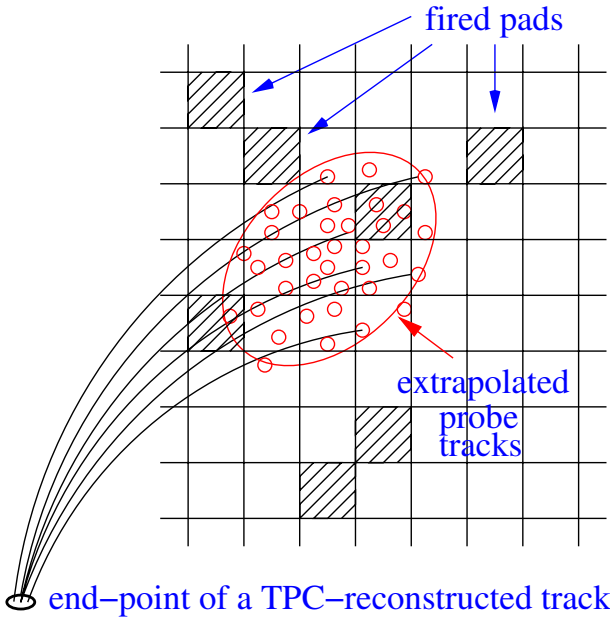

Fig. 3. A schematic view of the probe tracks extrapolated to the TOF surface.

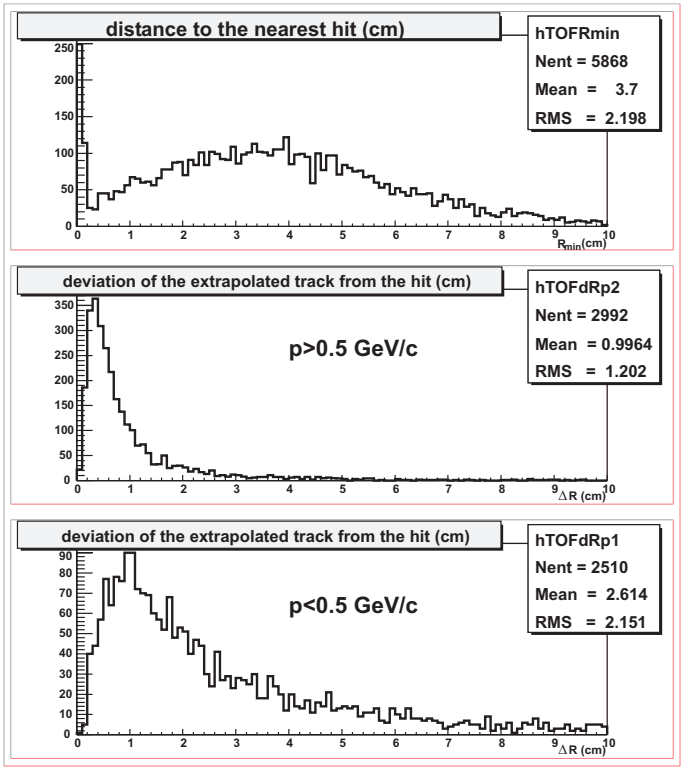

Fig. 4. R_{min} and ΔR distributions for one SHAKER event at $B = 0.2$ T.

charge induced on the pad, so that its resulting weight is: $weight = weight_1 \times weight_2$.

For a given TPC track, we have then a set of TOF pads and TOF dead regions crossed by the probe tracks. A TPC track may be matched with a dead region when none of the pads crossed by the probe tracks has fired and when the number of probe tracks crossing the dead region is larger than the number relative to the non firing pads. Otherwise, the track is matched with a pad. For each TOF pad a total weight is defined as the sum of the weighting contributions from all the probe tracks that cross it. The pad with the largest weight is chosen to be the TOF match for the TPC track. Notice that since tracks are curled in the magnetic field and may sometimes spiral this match is chosen as a first-crossing match on the TOF surface, for each track.

It is interesting to consider, in a qualitative way, the factors influencing the matching of tracks extrapolated from the TPC to the TOF with the corresponding fired pads. As already pointed out, this is a long distance extrapolation, from the TPC outer layer at 2.5 m radius up to the TOF surface at 3.7 m. Let us assume that the hit point (first crossing) of a track on the TOF sensitive surface could be exactly determined, i.e. without multiple scattering or any other source of extrapolation uncertainty. Let us call this point an "ideal" hit point. On the other hand, if we consider the realistic tracking of a particle from the TPC to the TOF, as performed by GEANT3, we obtain a "real" hit point (more than one in case of multiple crossing). The success of the track matching depends then on the ratio $< \Delta R > / < R_{min} >$, where ΔR is the deviation of the real hit point (first crossing) of a track from the corresponding ideal hit and R_{min} the minimum distance of this real hit with respect to all the other real ones (first or successive crossings) present on the TOF surface. ΔR is determined by the multiple scattering from the TPC to the TOF while R_{min} depends on the TOF occupancy. The lower the ratio, the better will be the matching efficiency.

Figure 4 shows the R_{min} and ΔR distributions relative to one SHAKER event at $B = 0.2$ T. This figure has been obtained with primary and secondary particles from the central region ($|\theta - 90°| < 45°$) tracked in the TPC. The narrow peak at $R_{min} \approx 0$ corresponds to δ-ray background. The fraction of tracks with $\Delta R > R_{min}$ is $\approx 25\%$. Without the TRD [7] in between the TPC and the TOF, this fraction decreases by a factor ≈ 0.8. In principle tracks with $\Delta R > R_{min}$ cannot be correctly matched and will presumably have a wrong time assignment.

The momentum acceptances of the various steps of the TPC-TOF matching procedure are shown in Figs. 5 and 6 for primary particles of different species[3] generated in the $|\theta - 90°| < 45°$ region, together with the original particle momentum spectra. The areas between the dashed/dotted-line histograms of Figs. 5 and 6 represent the corresponding acceptance losses. The loss "without TPC tracks" refers to particles not reconstructed in the TPC, entering the TPC dead space or decaying/interacting before or inside the TPC; the loss "out of geometry" refers to extrapolated TPC tracks missing the TOF surface; the loss "dead space" refers to extrapolated TPC tracks ending up in the TOF dead space (between neighbouring

[3] "Primary" electrons and positrons are originated from the decay chains of primary neutral pions.

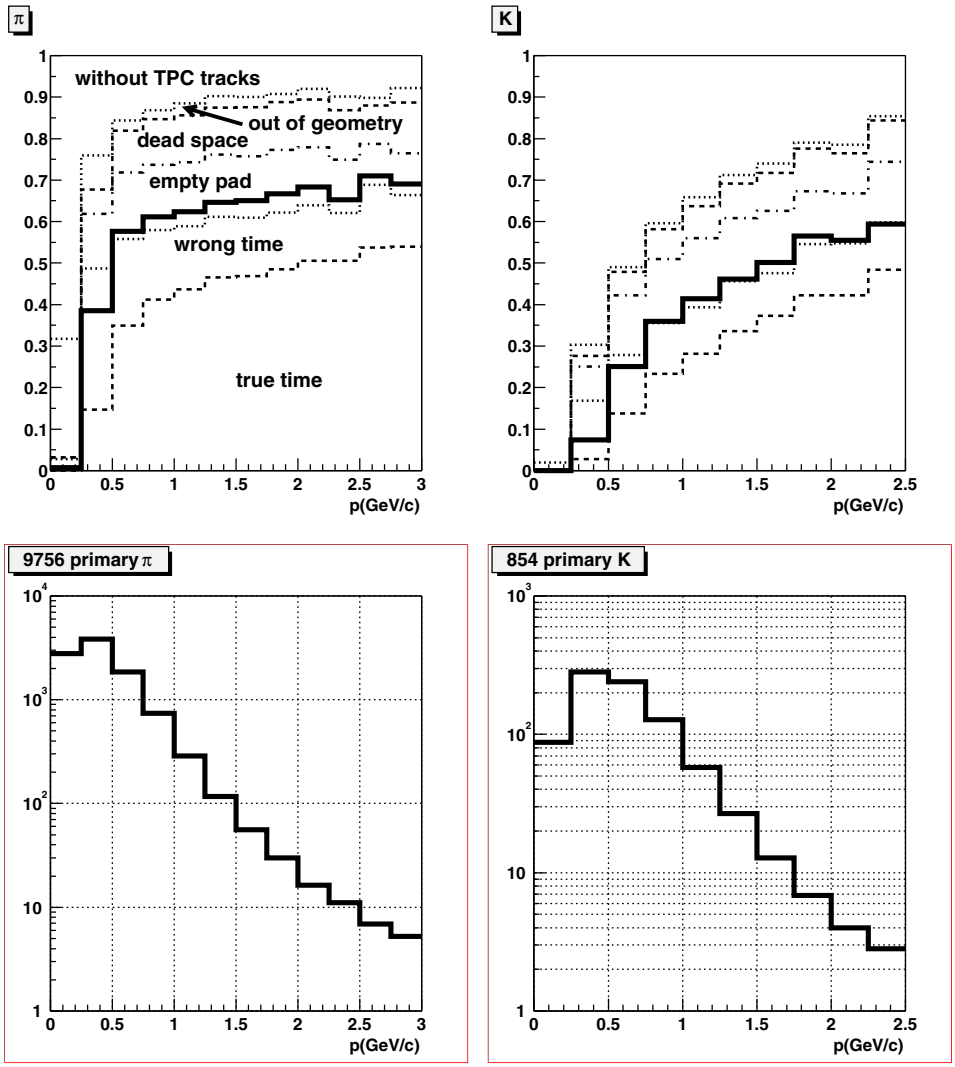

Fig. 5. Acceptances (upper, dashed/dotted-line histograms) of primary $\pi^{\pm}$ (left) and $K^{\pm}$ (right), as functions of momentum, for (from top to bottom): a) tracking in the TPC, b) extrapolation to the TOF surface, c) extrapolation to the TOF sensitive-pad surface, d) matching with the fired TOF pads, e) correct matching with the fired TOF pads. The solid-line histograms superimposed refer to primary particles "really" hitting the TOF sensitive surface. All the acceptances are normalized to the original samples of primary particles generated in the $|\theta - 90°| < 45°$ region (100 HIJING events at $B = 0.4$ T). The single-event momentum spectra (lower histograms) refer to these originally generated primaries.

strips, for example); the loss "empty pads" refers to extrapolated TPC tracks impinging on TOF pads which have not fired (mostly because of particle decays and interactions between the TPC and the TOF); the loss "wrong time" refers to extrapolated TPC tracks matched with pads fired by other tracks. The "true time" acceptance in Figs. 5 and 6 refers to extrapolated TPC tracks well matched with the pads they have actually fired.

One can see from these figures that in the momentum range $p > 0.5$ GeV/c the fractions of tracks matched with fired pads ("true time" + "wrong time" areas) correspond to the fractions of originally generated particles (i.e. "real" particles) actually hitting the TOF sensitive surface (solid-line histograms). It should be pointed out that for electrons the loss "without TPC track" is considerable as a consequence of their much softer momentum spectrum.

Let us define the TPC-TOF matching efficiency, for each type of particle, as:

$$efficiency = \frac{N^t_{match}(i)}{N(i)}$$

where $N(i)$ is the total number of particles of type i (with $i = \pi$, K, p) extrapolated to the TOF sensitive-pad surface and $N^t_{match}(i)$ is the number of correctly matched particles (with "true time") of the same type. This efficiency corresponds to the ratio of the areas below histograms e) and c) in Figs. 5 and 6, for each kind of particle. The results obtained with 100 HIJING-generated events

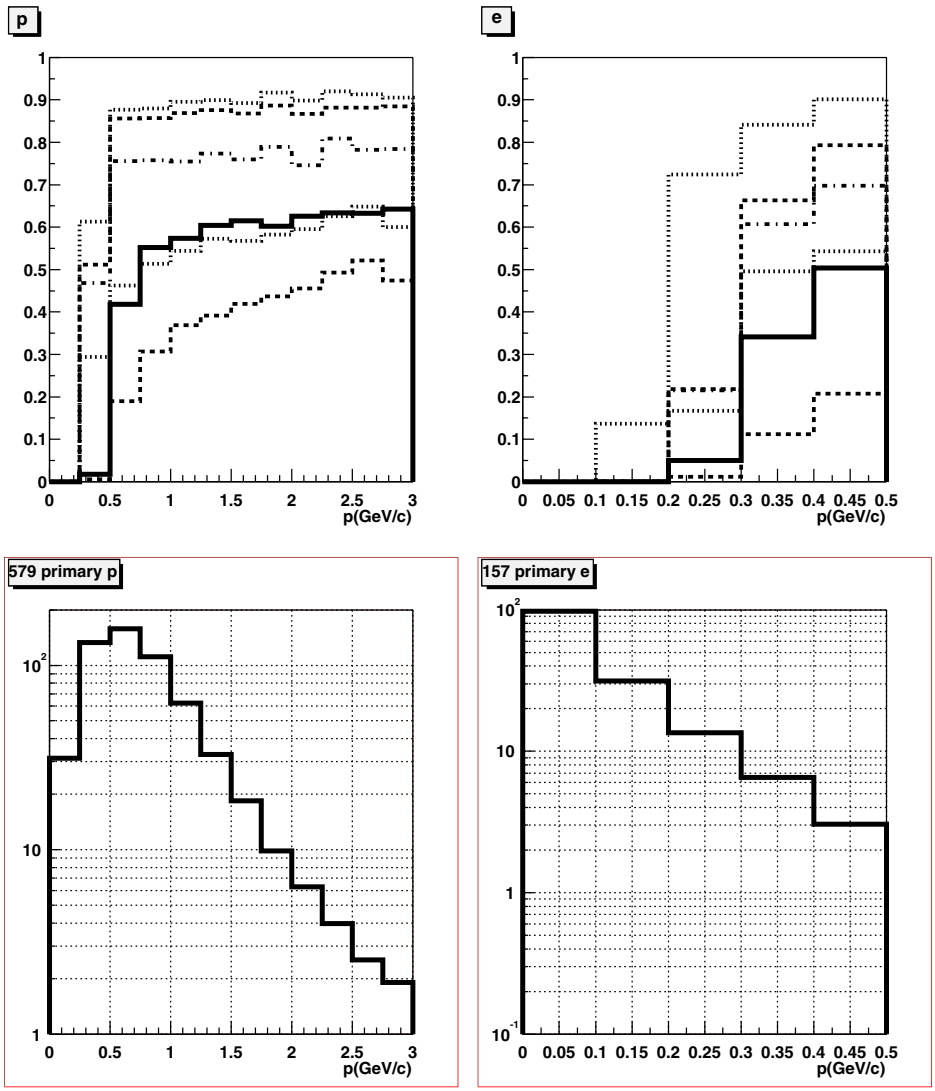

Fig. 6. Same as Fig. 5 for primary p($\bar{\text{p}}$) and $e^{\pm}$.

are summarized in Table 1 for two different magnetic field values: $B = 0.2$ T and $B = 0.4$ T. As one can see in this table, only the pion efficiency increases when B increases. This is due to the fact that only the TOF acceptance for low-momentum pions (with $p < 0.5$ GeV/c) is sizeably reduced when going from 0.2 to 0.4 T (see later on Table 2). These soft pions, which mostly contribute to the "wrong time" sample at $B = 0.2$ T, do not reach the TOF at $B = 0.4$ T. As a consequence, the pion efficiency improves. Using SHAKER, all the efficiencies in Table 1 are a few percent higher due to the slightly harder particle momentum spectra produced by this generator [3,4,5]. If the TRD is not included as passive material between the TPC and the TOF, the pion and kaon efficiencies both increase by a factor ≈ 1.3, and the proton efficiency by a factor ≈ 1.6 (thus becoming equal to the pion efficiency).

As anticipated, the number of probe tracks generated for each TPC "mother"-track plays a role in the TPC-TOF matching procedure. When going from $\text{N}_{\text{probe}} = 1$ to $\text{N}_{\text{probe}} = 20$ (the present value), the matching efficiency improves by a factor ≈ 2. Meanwhile the percentage of TPC tracks matched with "empty pads" decreases by a factor ≈ 3 and the percentage corresponding to "wrong time" pads increases up to a level which fits the TOF occupancy caused by background hits, as it should be. Hence no significant improvement can be obtained for $\text{N}_{\text{probe}} > 20$.

Table 1. TPC-TOF matching efficiencies (%) for primary hadrons extrapolated to the TOF sensitive-pad surface with $B = 0.2$ T and, in brackets, with $B = 0.4$ T (100 HIJING events).

Primary hadron	Efficiency
$\pi^{\pm}$	38 (42)
$\text{K}^{\pm}$	37 (36)
p($\bar{\text{p}}$)	35 (32)

3 Particle identification

Using the tracking and timing information particle identification (PID) may be performed. Different methods can be adopted for this PID task. In this section we will describe a "contour method" (where the contour is formed by a number of straight lines in the mass-momentum plane to define the PID selection region), and a "probability method".

3.1 Contour method

For this method all TPC reconstructed and TOF matched primary particles are entered in a momentum versus mass plot as shown in Fig. 7 for SHAKER "à la RHIC"[4] events. Negative mass values correspond to negative square-root arguments in the mass determination formula:

$$m = p(t^2/l^2 - 1)^{1/2} \quad (1)$$

p, t and l being the particle momentum, time-of-flight and track length. The mean flight-time for primaries from the $|\theta - 90^\circ| < 45^\circ$ region reaching the TOF is ≈ 16 ns, and the mean flight-length ≈ 4.2 m, with $B = 0.2$-0.4 T.

Notice that in this plot we have all the particles associated with fired TOF pads. Tracks matched with multihit pads have been included here in order to check the full particle identification power of the detector, as we will see later on. We observe distinct clusters of points corresponding to pions, kaons and protons as well as a horizontal broad band which corresponds to mismatched tracks, with pads giving "wrong times" (see Sect. 2). This leads to contamination, even in the low momentum region where the mass resolution ($\partial m/m$) is good. At larger momenta, the particle clusters become obviously wider because the mass resolution ($\partial m/m$) increases with the particle momentum[5] even for practically constant time resolution ($\partial t/t$). Moreover, at small momenta, the particle clusters appear to be systematically distorted, i.e. curved towards larger masses. The reason is that we calculate the mass assuming that the particle momentum is constant, i.e. the same as at the production vertex, whereas it decreases due to energy loss when the particle travels all the way to the TOF. One can reduce this effect by using in the mass calculation some effective momentum corresponding to the middle-point of the track, instead of the momentum at the vertex.

[4] Since it is obvious that the overall PID efficiency and contamination will indeed depend on the particle momentum spectra, we have made the exercise to modify the SHAKER generation parameters in order to approximately reproduce the recent experimental data on the inclusive π, K, p distributions from RHIC [16].

[5] The $\partial m/m$ resolution has three main contributions: i) $\partial m/m = \partial p/p$; ii) $\partial m/m = (E/m)^2 \partial t/t$; iii) $\partial m/m = (E/m)^2 \partial l/l$. At relatively high momenta, it is mainly driven by the errors on time-of-flight and track length rather than by the errors on the momentum determination.

For the identification procedure we introduce specific contour cuts, shown in Fig. 7, for kaons and protons. The shape of the contours is dictated by the concern to extend the range of pure identification to the largest momenta, even at the expense of efficiency. Figure 7 shows two different choices of the kaon contour cut. Unless differently specified, the kaon contour cut corresponding to the narrower (m, p) region has been used as default cut in the following.

Besides these graphical cuts, in the PID procedure described herein, different matching cuts were applied to different particle species. The strongest matching cuts were applied to kaons (because of the large pion contamination): only unambiguous correspondences between tracks and TOF pads were selected, i.e. only pads matched with single tracks. For protons, pads matched with more than one track were also considered since we expect one half of these tracks to have "true time" and the other half to be outside the PID contour cuts. Unless differently identified (as kaons or protons), all the other TPC-reconstructed primaries, matched or mismatched with the TOF, were regarded as pions. This does not lead to a very large contamination due to the overwhelming percentage of pions in the SHAKER and HIJING events [3]. Of course a pion contour cut may also be defined, as for kaons and protons, whenever an increased purity of the pion sample is needed. For Pb-Pb collisions we do not consider any contour cut for attempting electron identification (below say 0.5 GeV/c) since the pion contamination is prohibitive in this case.

3.2 PID efficiency and contamination

Let us call $N_{id}(i)$, with $i = \pi$, K, p, the number of identified hadrons of different species according to the criteria specified in Sect. 3.1. This number is obviously $N_{id}(i) = N^t_{id}(i) + N^w_{id}(i)$, where $N^t_{id}(i)$ is the number of well identified particles of type i and $N^w_{id}(i)$ the number of non-type i particles misidentified as particles of type i. The efficiency and contamination of the PID procedure, for each type of particle, are then:

$$\textit{efficiency} = \frac{N^t_{id}(i)}{N(i)}, \qquad \textit{contamination} = \frac{N^w_{id}(i)}{N_{id}(i)}$$

where $N(i)$ is the total number of particles of type i present in the (m, p) scatter-plot, i.e. of TPC-reconstructed and TOF-matched primary particles. The momentum dependence of the PID results is presented in Fig. 8 for 100 HIJING events at two different magnetic field values: $B = 0.2$ T and $B = 0.4$ T, separately for π, K and p. This figure characterizes the performance of the method itself. One can see that the π, K, p contaminations obviously increase with momentum when approaching the limits due to time resolution. For kaons and protons, the contaminations also increase at low momenta as a consequence of TPC-TOF track mismatching due to the severe background conditions (see Sect. 3.1). Finally, the effect of the larger magnetic field intensity is almost negligible at this stage.

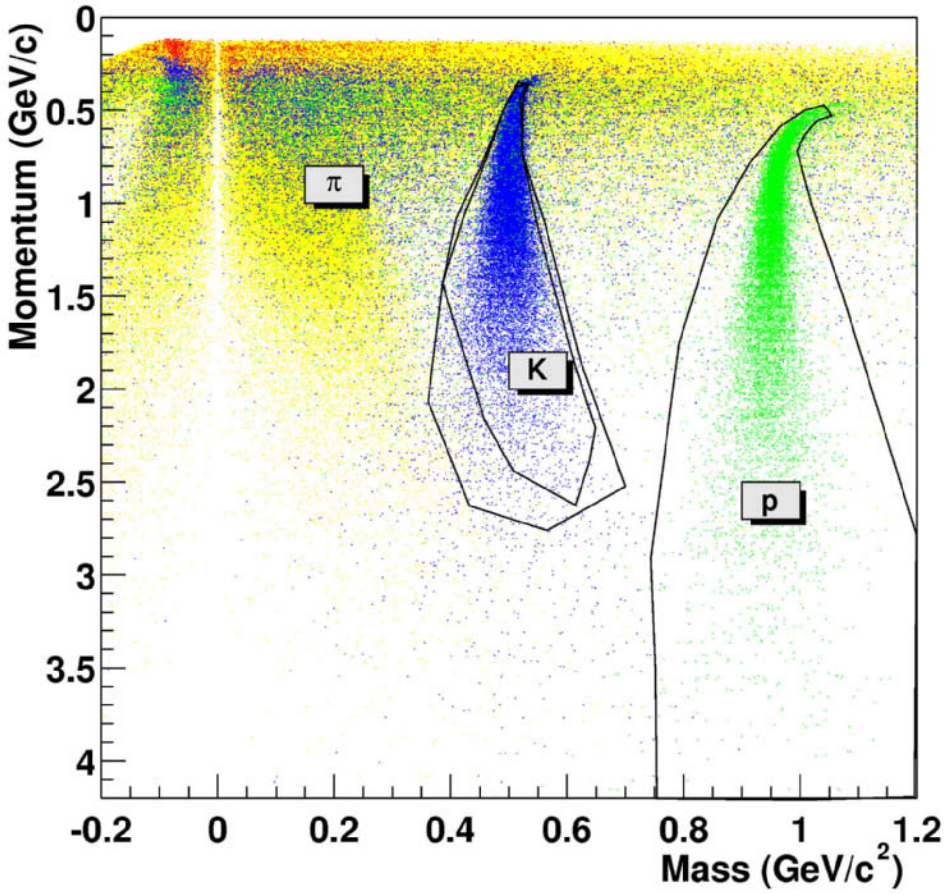

Fig. 7. Mass separation with the TOF detector (overall time resolution: 120 ps) as a function of momentum for 25 SHAKER "à la RHIC" events, with B=0.2 T.

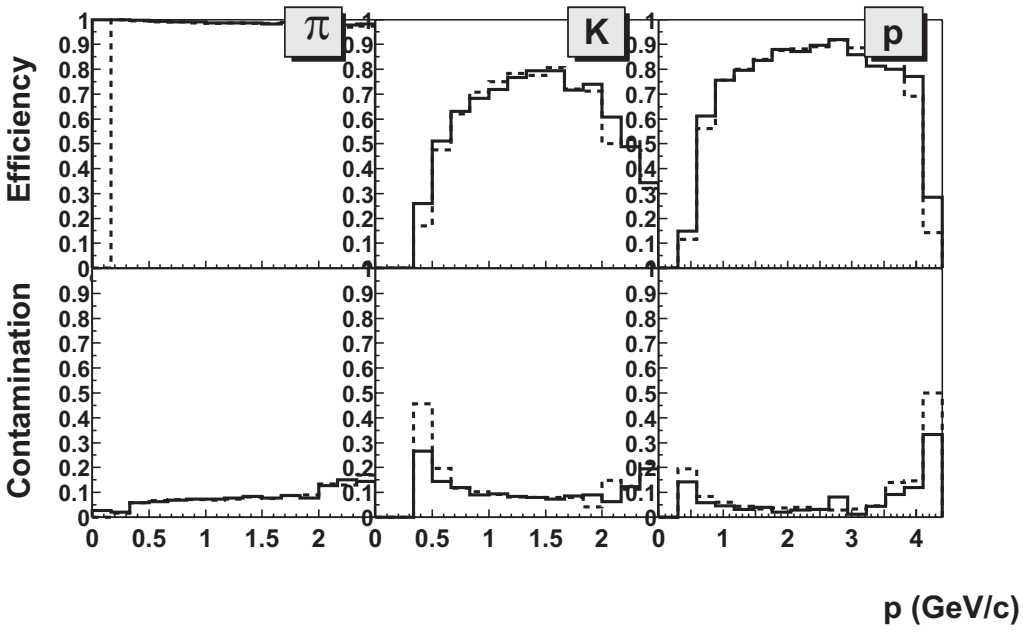

Fig. 8. PID efficiencies and contaminations vs. momentum for primary charged particles of different species matched with fired TOF pads (100 HIJING events), tracked with $B = 0.2$ T (solid-line histograms) and $B = 0.4$ T (dashed-line histograms).

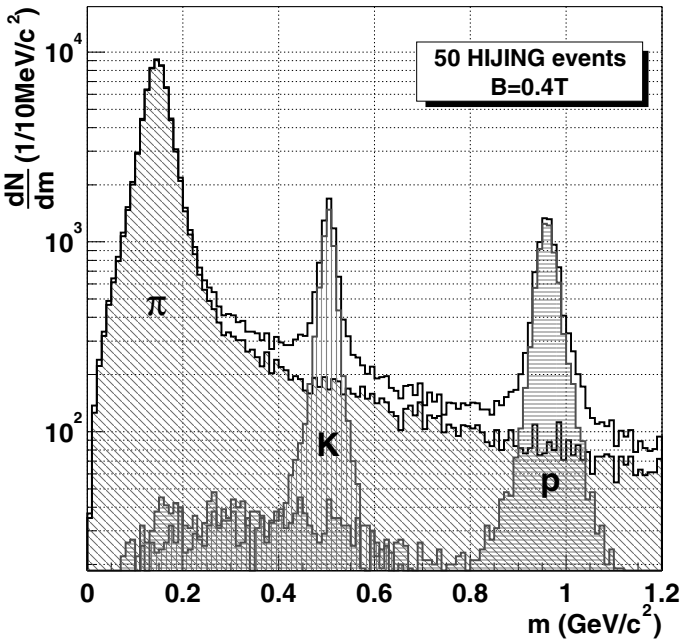

Fig. 9. Reconstructed mass with the TOF detector (overall TOF system resolution: 120 ps) in the momentum range 0.5 $\leq p \leq$ 2.5 GeV/c, for 50 HIJING events at $B = 0.4$ T. The grey- and dashed-area histograms superimposed show the individual mass distribution of the true pions, kaons and protons associated with the fired TOF pads.

Figure 9 shows the reconstructed particle mass[6] for TOF-identified primaries with momenta in the range $p =$ (0.5-2.5) GeV/c, where the achieved PID quality in terms of π/K/p separation clearly shows up.

Figure 10 shows the final PID power of the TOF detector for pions, kaons and protons, expressed in terms of "overall efficiencies" which include all the acceptance and efficiency factors involved in the analysis. In this case $N(i)$ is the total number of primary hadrons of type i originally generated in the angular region $|\theta - 90°| < 45°$. In Fig. 10, two different contour cuts for kaons (see Fig. 7) have been applied to the SHAKER "à la RHIC" sample, thus showing how a better kaon efficiency is achievable, say for $p > 1.75$ GeV/c, at the cost of a limited contamination increase.

When folding in the inclusive particle momentum spectra, the results, integrated over the whole PID momentum interval, are given in Table 2 for the HIJING event generator. These results obviously depend on the event generator parameters (dN_{ch}/dy density, p_t spectra, K/π and p/π particle ratios, etc.) and the simulated experimental conditions (in the presence of different materials, magnetic field values, etc.). Notwithstanding the uncertainties at the present stage, we can confidently conclude that in each Pb-Pb final state the ALICE TOF detector will be able to identify thousands of pions, and hundreds of kaons and protons, with 10% or less contamination in the momentum range exceeding ≈ 2 GeV/c for kaons, and extending up to ≈ 4 GeV/c for protons.

[6] Tracks with negative mass values (see Sect. 3.1 and Fig. 7) are entered in Fig. 9 histogram at the corresponding $|m|$ values.

Table 2. Overall PID efficiencies (%) and contaminations (%) in different momentum (GeV/c) ranges, relative to all primary hadrons generated in the $|\theta - 90°| < 45°$ region (100 HIJING events), tracked with $B = 0.2$ T and, in brackets, with $B = 0.4$ T.
(*) [*Identified pions, kaons and protons have respectively:* $p \geq$ 0.15 (0.2), 0.25 (0.3) *and* 0.35 (0.4) GeV/c, *at* $B = 0.2$ (0.4) T.]

Primary hadron	Momentum range	Overall efficiency	Contamination
$\pi^{\pm}$	(*) $p < 2.5$	63 (48)	7 (9)
$K^{\pm}$	(*) $p < 2.5$	14 (13)	13 (15)
p($\bar{p}$)	(*) $p < 4.5$	27 (24)	5 (7)
$\pi^{\pm}$	$0.5 < p < 2$	74 (72)	11 (12)
$K^{\pm}$	$0.5 < p < 2$	23 (21)	11 (12)
p($\bar{p}$)	$0.5 < p < 2$	37 (33)	5 (7)

Proton-proton collisions are characterized by a much lower multiplicity and a consequently much lower background with respect to typical heavy-ion collisions, thus allowing us to be confident that a good particle identification will be achieved with the TOF detector during the LHC p-p running periods.

Let us present some results obtained with a sample of 6000 PYTHIA [12] events, corresponding to minimum bias p-p interactions at a centre-of-mass energy $\sqrt{s} = 14$ TeV. As for Pb-Pb collisions, all TPC-reconstructed and TOF-matched primary particles are entered in a momentum versus mass plot as shown in Fig. 11, where distinct clusters corresponding to electrons, pions, kaons and protons can be clearly seen. In Pb-Pb collisions, the identification of electrons was not considered because of an exceedingly high background level. In the present p-p analysis, we gain a significant PID efficiency for electrons in the $0.1 \leq p \leq 0.5$ GeV/c range.

In Fig. 12 we show the overall PID efficiency and contamination as a function of momentum, for e, π, K and p primary particles produced in the $|\theta - 90°| < 45°$ central region. The contour cuts defined for e, K and p in p-p events are drawn in Fig. 11 and clearly differ from those previously adopted in the Pb-Pb case. The final PID power of the TOF detector turns out to significantly improve in the p-p case thanks to the much reduced background conditions. In the previously mentioned momentum ranges (beyond to ≈ 2 GeV/c for K and up to ≈ 4 GeV/c for p), the PID efficiencies are higher and the contaminations lower, almost negligible for kaons and protons. Moreover some electron identification would indeed be possible (up to ≈ 0.5 GeV/c) with less than 10% contamination.

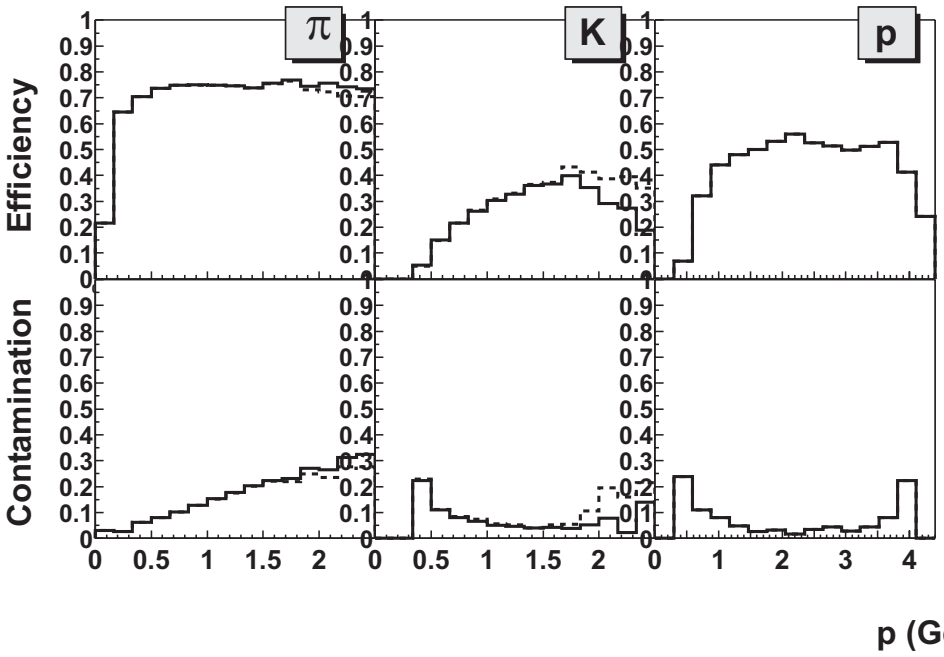

Fig. 10. Overall PID efficiencies and contaminations vs. momentum, relative to all primary charged particles of different species generated in the $|\theta - 90^\circ| < 45^\circ$ region (100 SHAKER "à la RHIC" events), tracked with $B = 0.2$ T: applying the narrower (solid-line histograms) and wider (dashed-line histograms) contour cuts shown in Fig. 7 for kaon identification.

3.3 Probability method

Another promising approach appears to be the so-called "probability method". It has already been used in the STAR experiment at RHIC [17]. For each kind of particle, one can derive a probability density function (p.d.f.) based on some separation parameter, for instance the mass, by fitting the appropriate Monte Carlo simulated distribution. We can then compute the probabilities for each TPC-TOF matched track, measured with a given mass m, to be a pion, a kaon or a proton (neglecting the electron case) from the heights of the corresponding mass p.d.f.'s (f_π, f_K, f_p) at this m-value. Each p.d.f. is normalized to the corresponding particle yield. The probability to be a particle of type i can be for instance defined as $P_i(m) = f_i(m)/(f_\pi(m) + f_K(m) + f_p(m))$. Examples of these f_i, for $i = \pi$, K, p, obtained as Monte Carlo mass distributions, are given in Fig. 13. Of course different sets of mass distributions should be simulated, corresponding to different appropriate momentum bins, in order to derive more accurate p.d.f.'s.

However mass is not a very good separation parameter because its probability density function has not a proper Gaussian shape as a consequence of the mass determination formula (1) given in Sect. 3.1. Time-of-flight is indeed Gaussianly distributed and can be more conveniently used for probability calculations. For a track measured with a given flight-time t, we can for instance calculate the probability to have a mass m_i, for $i = \pi$, K, p, as $P_i(t) = g(t_i)/(g(t_\pi) + g(t_K) + g(t_p))$, where $g(t_i)$ is the height of the Gaussian p.d.f. g (with mean value t and standard deviation σ_{TOF}) at the time t_i derived from the track length and momentum measurements with mass hypothesis m_i (see Fig. 14). Here a weighting procedure is applied to take into account the different particle yields.

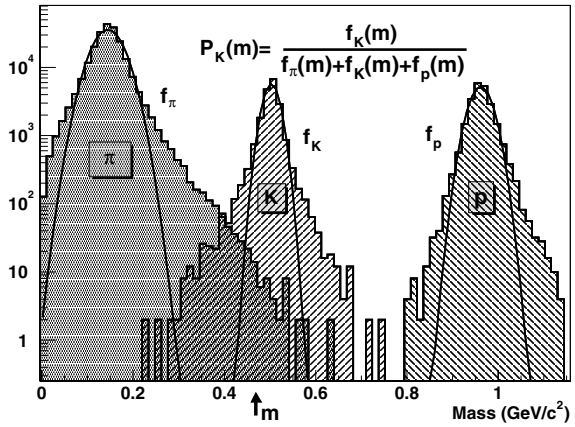

Fig. 13. Examples of mass probability density functions for pions, kaons and protons, obtained as mass spectra of unambiguously TPC-TOF matched primary tracks with $0.5 \leq p \leq 2.5$ GeV/c (100 HIJING events at $B = 0.4$ T). Superimposed, some Gaussian fits to guide the eye.

The time-based probabilities obtained in this way are shown in Fig. 15 as functions of the mass derived according to formula (1). One can see that the masses at which the probability for a particle to be a pion becomes equal to the probability to be a kaon (≈ 0.4 GeV/c^2), and the

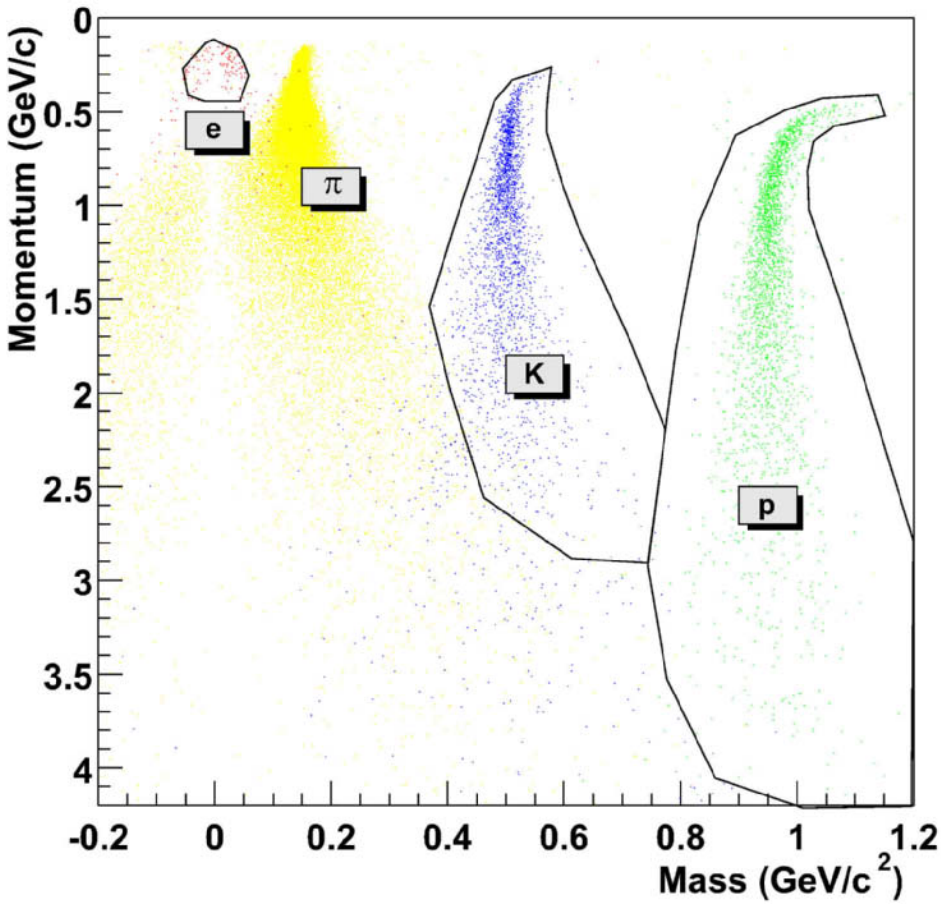

Fig. 11. Mass separation with the TOF detector (time resolution: 120 ps) as a function of momentum for 6000 p-p PYTHIA events, with $B = 0.2$ T.

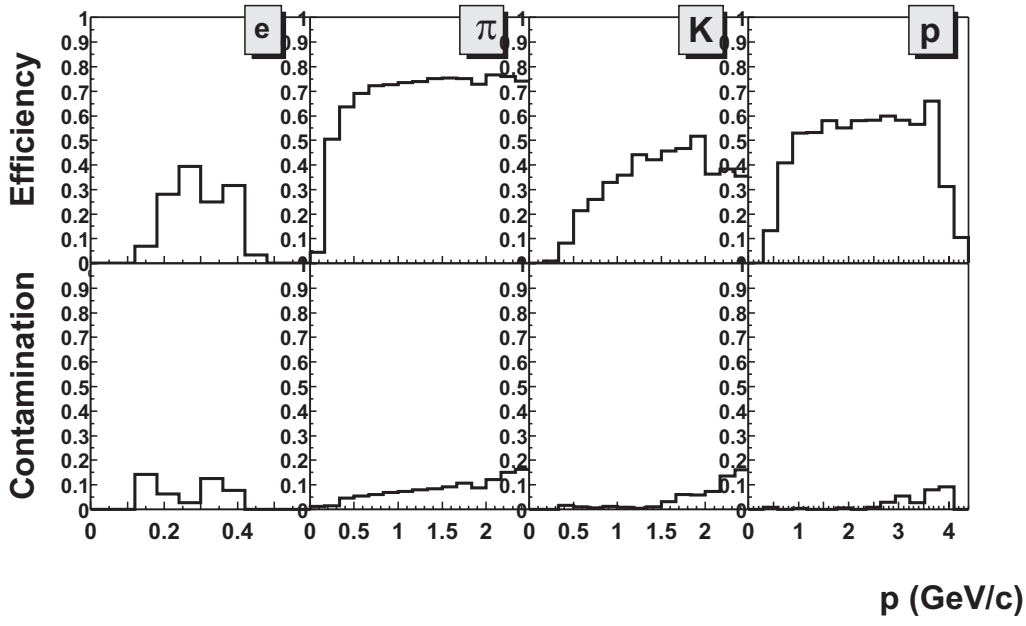

Fig. 12. Overall PID efficiencies and contaminations vs. momentum, relative to all primary charged particles of different species generated in the $|\theta - 90^\circ| < 45^\circ$ region (6000 p-p PYTHIA events), tracked with $B = 0.2$ T.

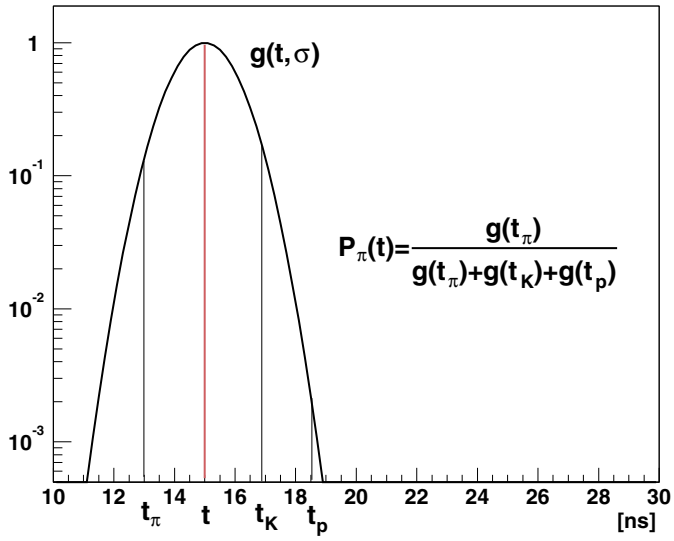

Fig. 14. Example of flight-time probability density function. The standard deviation σ_{TOF} of this Gaussian function, centred at the measured track time t, has been enlarged by an arbitrary factor for the sake of clarity.

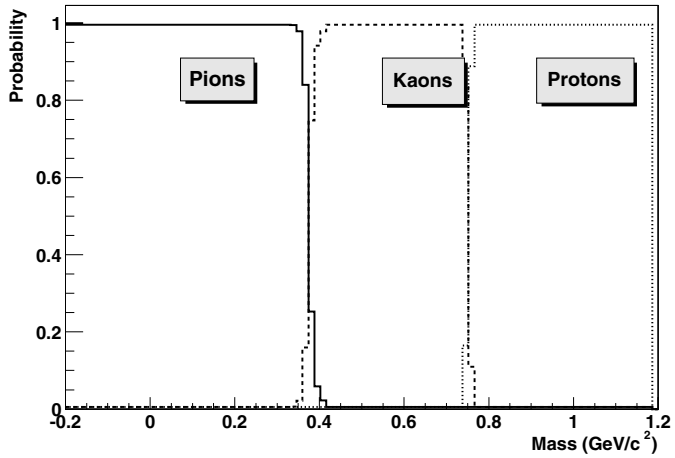

Fig. 15. Time-based PID probability distributions versus mass, for pions, kaons and protons, corresponding to unambiguously TPC-TOF matched primary tracks with $0.5 \leq p \leq 2.5$ GeV/c (50 HIJING events at $B = 0.4$ T).

probability to be a kaon becomes equal the probability to be a proton (≈ 0.8 GeV/c^2) correspond to the crossing points of the π, K, p mass p.d.f.'s of Fig. 13, as it should be.

It is important to underline that one can use such kind of information simultaneously from different ALICE sub-detectors providing PID: TOF (with time-of-flight), ITS and TPC (with dE/dx), HMPID [18] (with Čerenkov light), etc. By combining the different sub-detectors using multidimensional distributions, more accurate "global" PID probabilities could be derived. Another possible advantage of this approach is that PID probabilities are suitable to be introduced in the data analysis in a straightforward way, i.e. simply as weights (for instance, in invariant-mass spectra).

4 Conclusions

A procedure has been developed via Monte Carlo simulation to perform particle identification with the ALICE TOF detector in very challenging multiplicity and background conditions.

The initial step of the procedure described herein is the matching of the TPC-reconstructed tracks with the corresponding TOF elements. This is a lengthy extrapolation, across intermediate detectors and inside a magnetic field, hence a very delicate step which strongly depends on the experimental conditions (physics input and detector effects). The results, based on the "probe-track approach", are already satisfatory when tested in an extreme scenario (central Pb-Pb interactions at 5.5 TeV per nucleon pair and $dN_{ch}/dy = 8000$), thus proving the validity of this approach.

Concerning the final step, i.e. the effective PID procedure based on the time measurements from the TOF detector, two methods have been presented: i) a "contour method", applicable in case a two-dimensional treatment of the data in the mass-momentum plane is chosen; ii) a "probability method", applicable in case a single separation parameter (mass or time) is preferred. Both methods are of general validity. The PID efficiency and contamination have been shown to be very promising with a simple contour-cut approach thanks to the excellent efficiency and time resolution of the MRPC-strip technique adopted for the ALICE TOF implementation. It should be pointed out that PID efficiencies, contaminations and probabilities are model dependent, i.e. biased by the Monte Carlo physics input and, in particular, by the particle ratios. For instance if the number of kaons is much smaller than the number of pions, a 3 sigma separation does not necessarily mean a good kaon identification with low contamination because of a large tail of pions. However, if the model is reasonable, the PID performance can be reliably estimated. Later on our model will be compared with the experimental data and corrected, if needed.

Acknowledgements

This work has profited of the essential support of the Computer and Network Service of the Bologna INFN Section. We would also like to acknowledge the very helpful contribution of E. Ugolini (INFN, Bologna) and B. Sagliocca (University and INFN, Salerno).

References

1. ALICE Collaboration: Technical Proposal, CERN/LHCC/95-71
2. B. Alessandro et al.: ALICE Internal Note 2002-025
3. ALICE Collaboration: Time of Flight System, Technical Design Report, CERN/LHCC 2000-12, ALICE TDR 8, 16 February 2000
4. ALICE Collaboration: Answers to the Questions of LHCC Referees, CERN/ALICE, 5 May 2000

5. ALICE Collaboration: Addendum to ALICE TDR 8, CERN/LHCC 2002-16, 24 April 2002
6. ALICE Collaboration: Time Projection Chamber, Technical Design Report, CERN/LHCC 2000-001, ALICE TDR 7, 7 January 2000
7. ALICE Collaboration: Transition Radiation Detector, Technical Design Report, CERN/LHCC 2001-21, ALICE TDR 9, 3 October 2001
8. http://AliSoft.cern.ch/offline
9. R. Brun et al.: http://root.cern.ch
10. R. Brun et al.: GEANT3, CERN program library Q123
11. T. Sjöstrand: Comp. Phys. Commun. **39** (1986) 347.
12. H.-U. Bengtsson, T. Sjöstrand: Comp. Phys. Commun. **46** (1987) 43
13. X.N. Wang, M. Gyulassy: Phys. Rev. D **44**(1991) 3501; X.N. Wang, M. Gyulassy: Phys. Rev. D **45** (1992) 844; X.N. Wang, M. Gyulassy: Comp. Phys. Comm. **83**(1994) 307
14. ALICE Collaboration: Inner Tracking System, Technical Design Report, CERN/LHCC 99-12, ALICE TDR 4, 19 June 1999
15. F. Pierella: Study of The ALICE TOF detector performances and charm detection in Pb-Pb interactions at LHC, PhD Thesis, University of Bologna (2003)
16. K. Adcox et al.: PHENIX Collaboration, Phys. Rev. Lett. 88, 242301 (2002)
17. http://www.star.bnl.gov/comp/pkg/dev/StRoot /StPidAmpMaker/doc
18. ALICE Collaboration: High Momentum Particle Identification Detector, Technical Design Report, CERN/LHCC 98-19, ALICE TDR 1, 14 August 1998